UNCLASSIFIED

Generation of RF Radiation by Femtosecond Atmospheric Filaments

Travis Garrett | Research Physicist | AFRL/RDHEC | ICNSP 2019

Introduction

- Atmospheric filaments are famous as sources of THz radiation, which was hard to produce and detect until recent decades.
- Recent experimental work at the AFRL has detected and characterized the GHz RF radiation that is also produced by filaments.
- The existing theories that explain the production of THz radiation do not explain the distinct RF raditation: a new physical mechanism must be responsible.
- In our model the expansion of a hot outer shell of electrons from the plasma column drives longitudinal currents that generate the RF.

Laboratory Filament Measurements

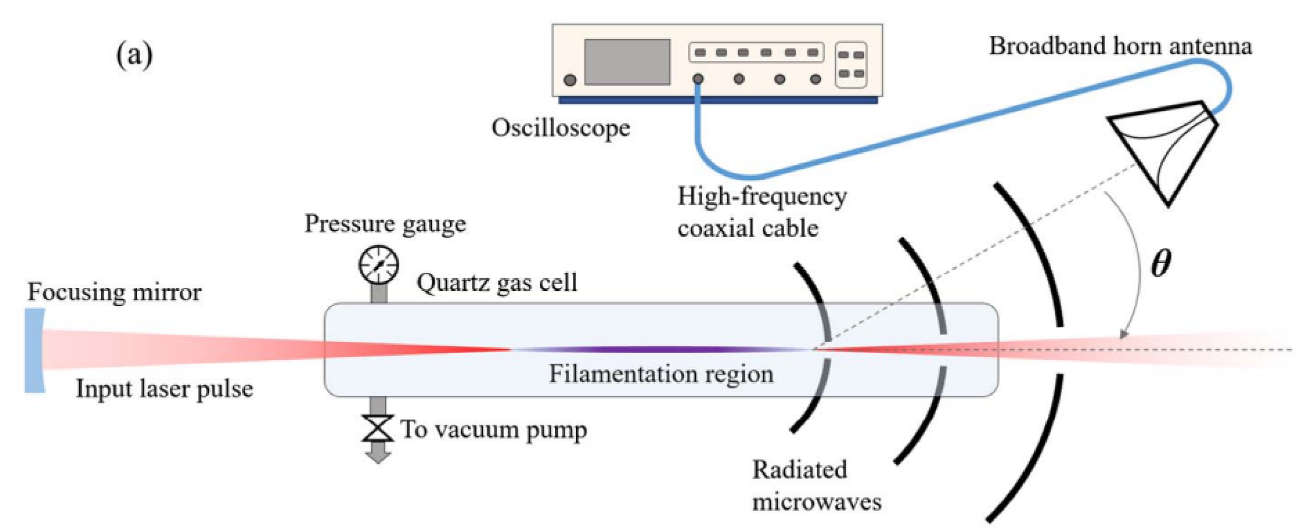

Figure 1: USPL shots are focused to produce filaments within a gas cell at different pressures. The resulting RF is then measured at varying angles in the far field. [1].

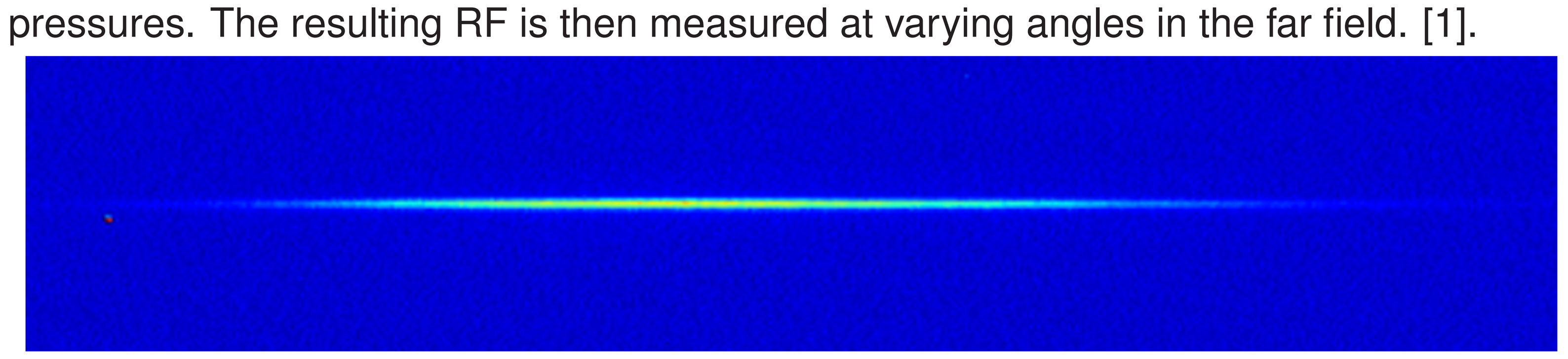

Figure 2: Heat map plot of $\sim$ 25 cm USPL filament plasma generated from a 27 mJ pulse at an air pressure of 2 Torr (ICCD camera with 200 ns shutter time).

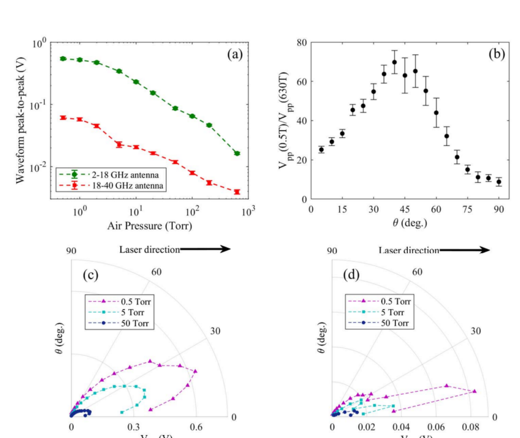

Figure 3: Like THz radiation the RF forms a radially polarized conical shell around the laser propagation direction [2]. However the amplitude of the RF grows strongly with decreasing pressure.

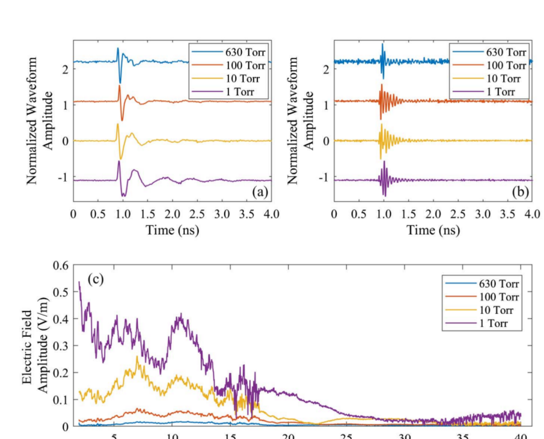

Figure 4: The FFTs at different pressures have roughly similar profiles, and show a broad peak around $10GHz$.

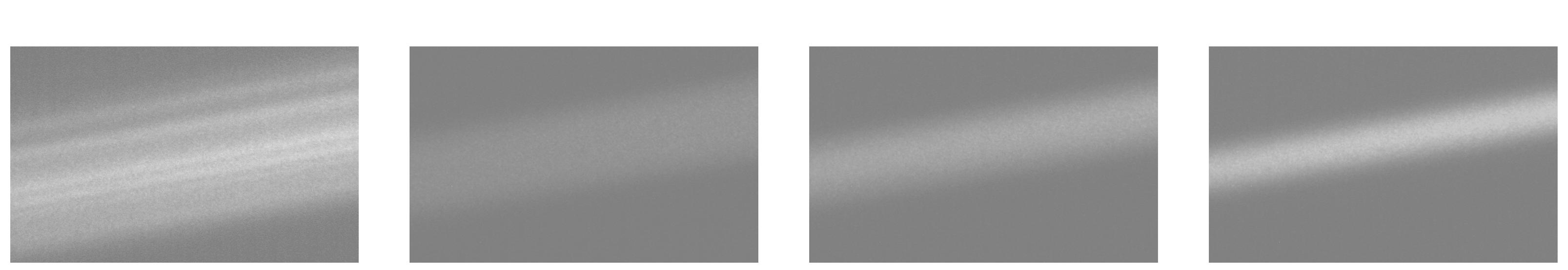

1 atm | 100 Torr | 10 Torr | 1 Torr

Microscope images of multiple filaments at atmospheric pressure and large filaments at 100, 10 and 1 Torr from a 40 mJ pulse.

Numerical Modeling

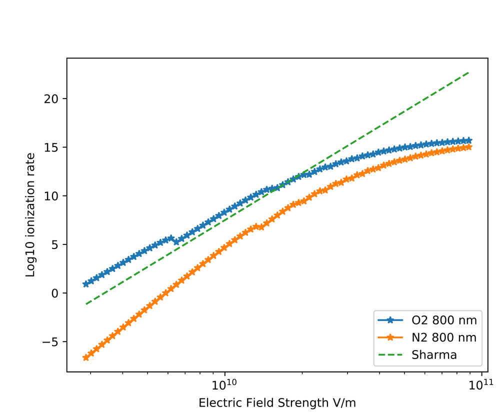

Figure 5: The ionization rates for O2 and N2 at $800nm$ are calculated using [3]. Recent experimental measurements [4] for O2 match closely near $E \sim$ 2E10 V/m.

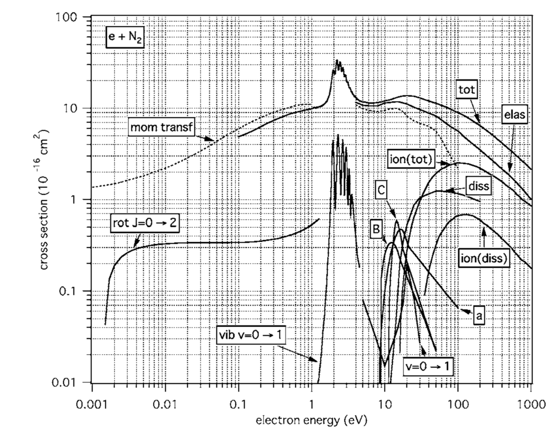

Figure 6: Assorted elastic and inelastic e-N2 cross sections. Elastic collisions are most important on short time scales, and the $2-3eV$ peak is relevant.

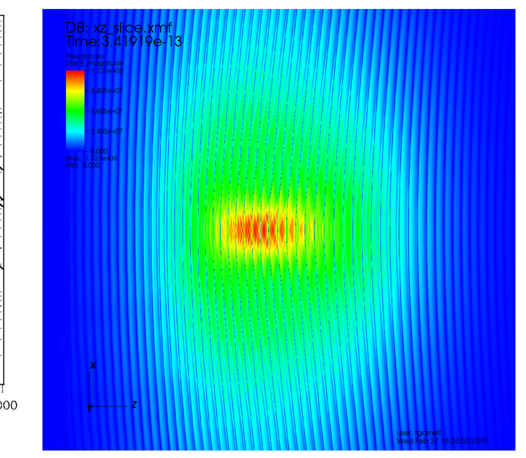

Figure 7: ICEPIC simulation of Kerr focusing in a $800nm$ pulse, using a Pade approximation to invert $\vec{D} = (\epsilon + \chi^3|E|^2)\vec{E}$.

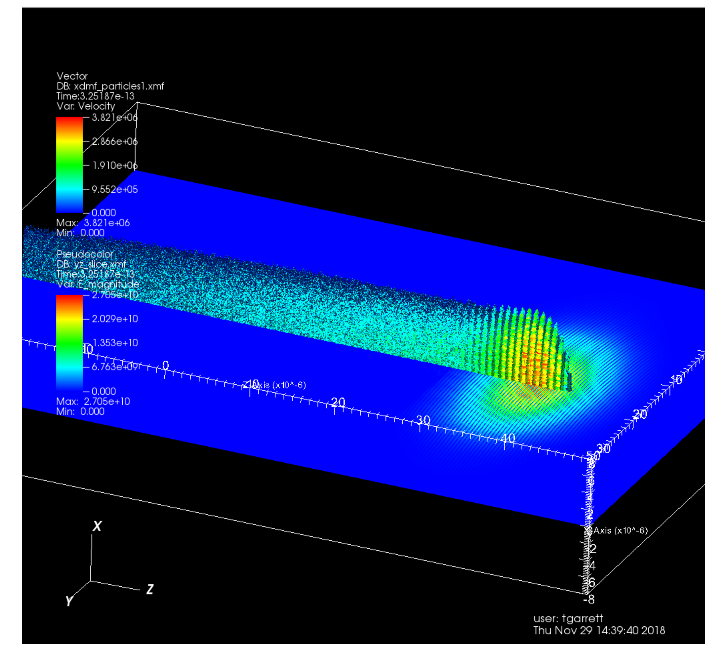

Figure 8: ICEPIC simulation of $800nm$ hard focus filamentation using the Kerr nonlinearity, multiphoton ionization and a moving window. Slices of the electron velocities and electric field strength are shown.

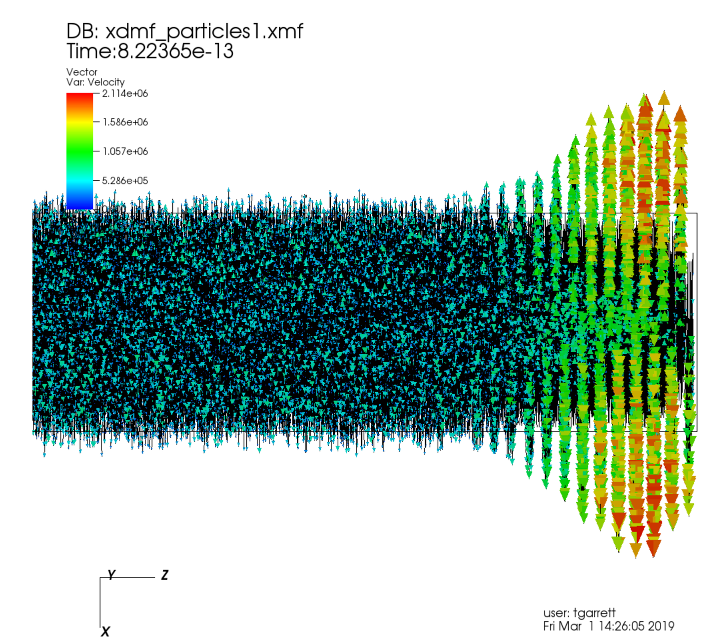

Figure 9: Close view of the electron velocities. The largest residual kinetic energies are in the $2-3eV$ range for a pulse with an envelope of $E \sim$ 2E10 V/m.

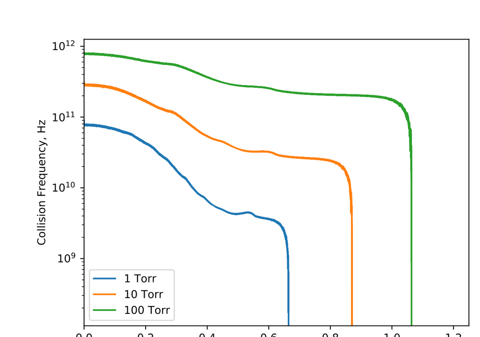

Figure 10: Collision frequencies inside filaments at 1, 10, and 100 Torr.

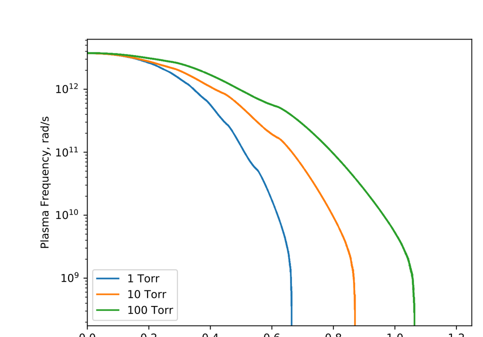

Figure 11: Plasma frequencies for the 1, 10 and 100 Torr filaments.

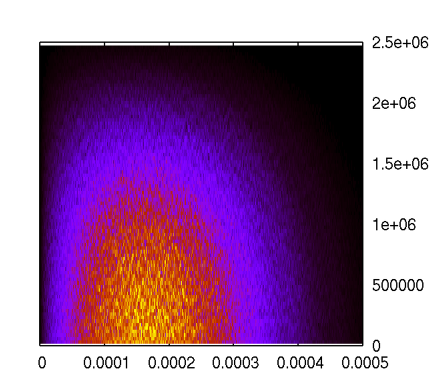

Figure 12: Histogram of initial residual electron velocities at 1 Torr.

References

[1] Englesbe, A., et al. Gas pressure dependence of microwave pulses generated by laser-produced filament plasmas. *Optics letters*, 43.20, 2018.

[2] Amico, C. D., et al. Forward THz radiation emission by femtosecond filamentation in gases: theory and experiment. *New Journal of Physics*, 10.1, 2008.

[3] Popruzhenko, S. V., et al. Strong field ionization rate for arbitrary laser frequencies. *Phys Rev Lett*, 101.19, 2008.

[4] Sharma, A., et al. Measurements of Electron Numbers in Femtosecond Laser Induced Plasmas Using Rayleigh Microwave Scattering. *2018 AIAA Aerospace Sciences Meeting*., 2018.

Numerical Modeling cont.

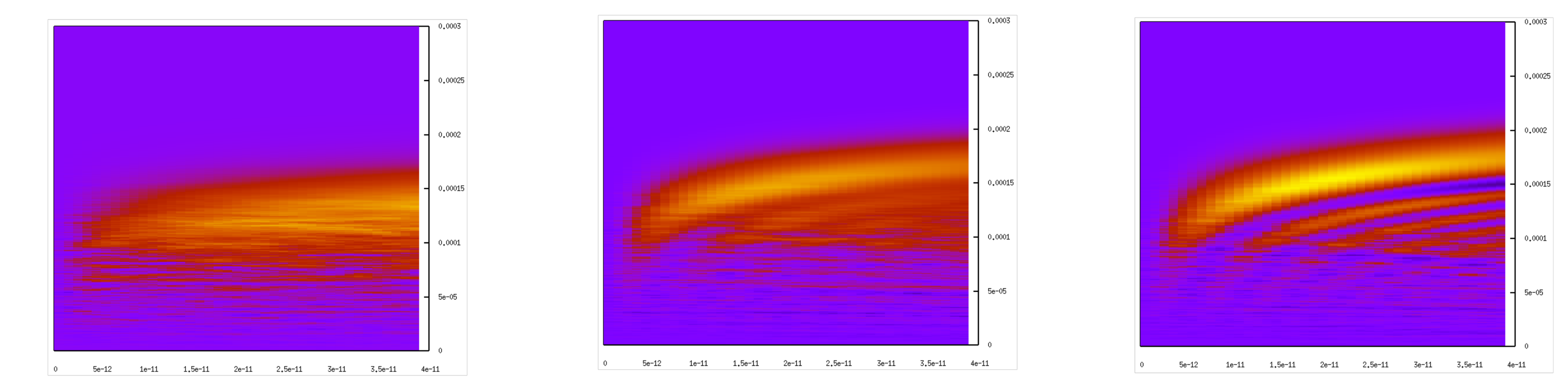

100 Torr | 10 Torr | 1 Torr

Charge separation over 40 ps in a PIC simulation of a cylindrical slice of a plasma column at 100, 10, and 1 Torr. The transverse expansion of the hot outer electrons is limited more by the mean free path at higher pressures, and by electrostatic forces at low pressures.

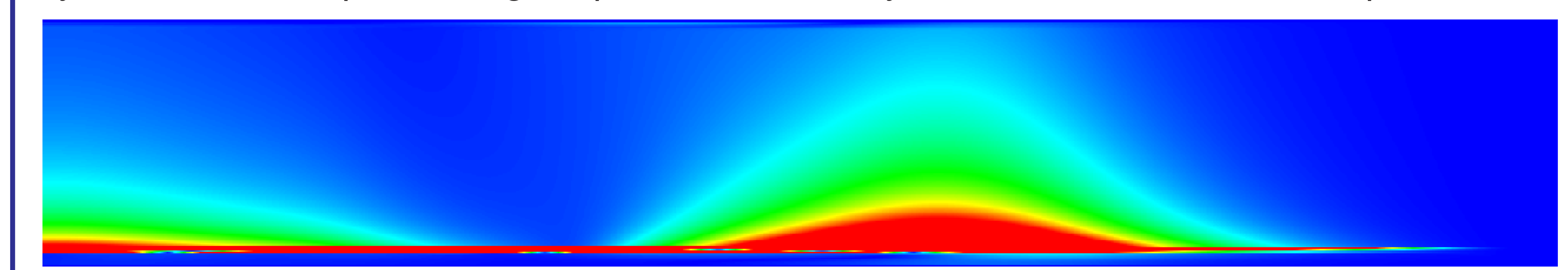

Figure 13: Axisymmetric ICEPIC simulation of the electric field strength near the plasma column. The varying transverse currents found in the electrostatic simulations drive longitudinal currents within the plasma (with the Drude model: $\epsilon(\omega) = (\epsilon_0\omega_p^2)/(i\nu_c\omega - \omega^2)$ implemented via an auxiliary differential equation).

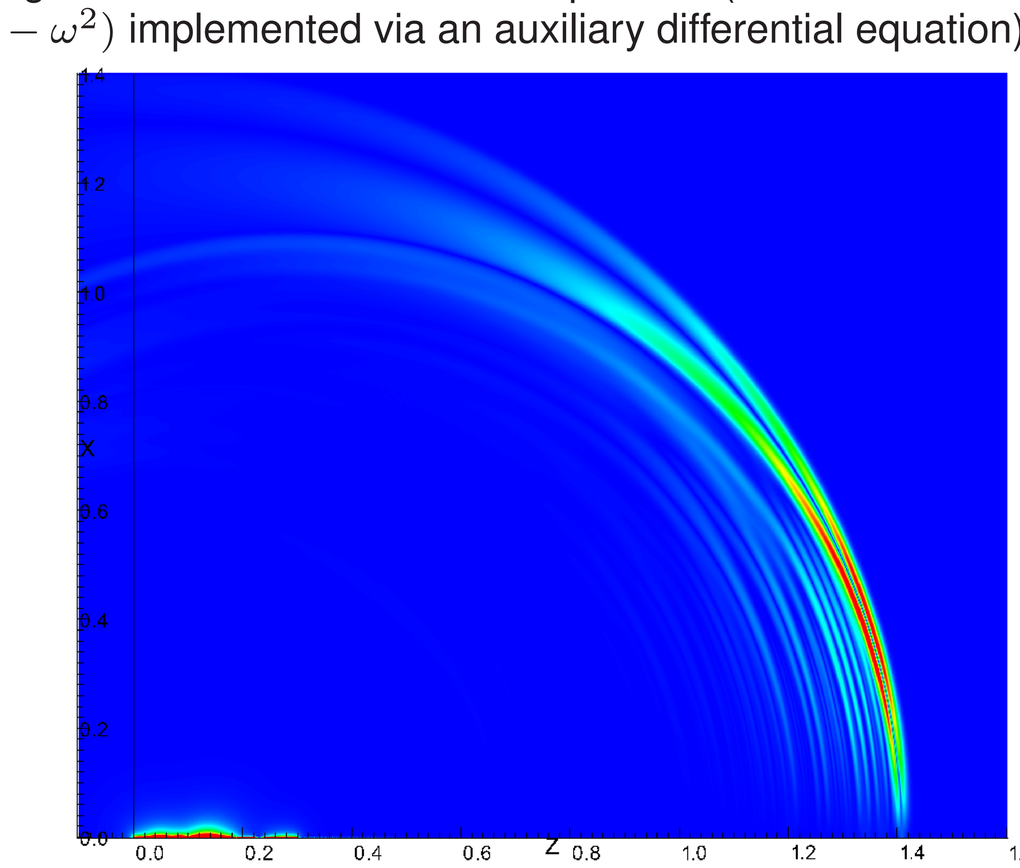

Figure 14: Electric field strength in a large scale axisymmetric simulation of the RF pulse produced by the longitudinal currents found in the previous simulation. Fields from the residual return currents inside the filament can also be seen at the bottom left.

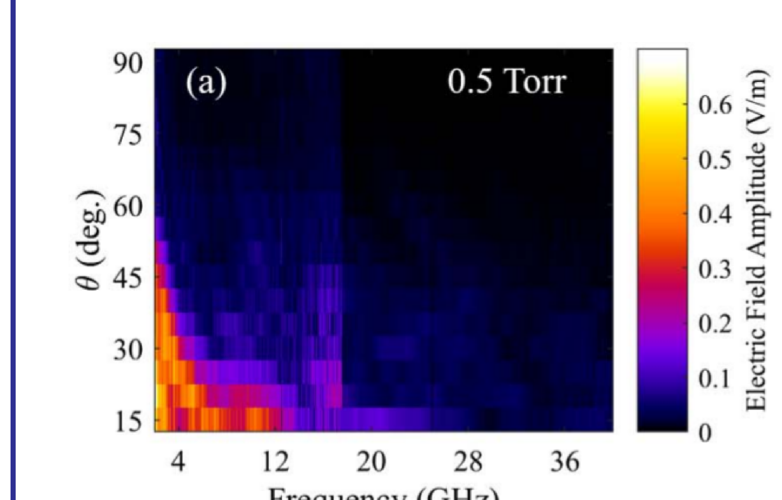

Figure 15: Frequency spectra as a function of angle for the RF measured in the lab at 1.2m from the filament (at 0.5 Torr).

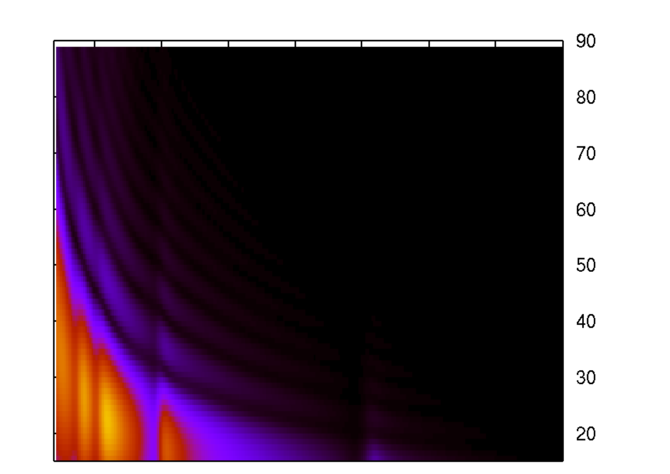

Figure 16: FFTs as a function of angle for the simulated RF at 0.5 Torr. The field strength also closely matches the $\sim$ 0.5 V/m experimental value.

Distribution Statement